WALL-FUNCTION STRATEGIES FOR USE IN TURBULENT FLOW CFD

T J Craft, S E Gant, A V Gerasimov, H Iacovides, B E Launder
Mechanical, Aerospace & Manufacturing Engineering Department,
UMIST, Manchester, UK

Abstract

For CFD calculations of turbulent flow near smooth walls, two broad strategies are used to resolve the very influential, very complex and very thin near-wall viscosity-affected sub-layer. Either one uses a fine numerical mesh and a turbulence model that (supposedly) accounts for viscous influences; or one employs "wall functions" – overall formulae that attempt to take account of the resistance of the sublayer to the transport of momentum and heat. The latter may require only one-hundredth of the computational effort of the former and are thus strongly favoured for industrial calculations. The track record of such schemes is poor, however, partly because of inappropriate implementation and partly because the schemes themselves have inherent limitations.

The present paper reviews the evolution of wall-function strategies since the 1960's. Attention is then given to two new schemes evolved by the authors, one based on an analytical treatment and the other on a numerical resolution of the near-wall sub-layer. Several recent applications are shown of mixed and forced convection.

1 Introduction

In most practical problems of convective heat transport to or from a rigid surface, the flow in the vicinity of the body is in turbulent motion. However, at the solid-fluid interface itself, the no-slip boundary condition ensures that turbulent velocity fluctuations vanish. Thus, at the wall, diffusive transport of heat and momentum in the fluid is precisely expressible by the laws applicable to laminar flow. Indeed, because the turbulent shear stress and, often, the turbulent heat flux can, by continuity, increase only as the cube of the distance from the wall, there is a thin but very important sub-layer immediately adjacent to the solid surface where the transport of heat and momentum is predominantly by molecular diffusion. As one moves further from the wall, again by virtue of the cubic variation, there is a very rapid changeover to a state where turbulent transport dominates, a condition that normally prevails over the remainder of the flow. This thin sub-layer and the adjacent transition region extending to the fully turbulent regime – what collectively we shall term the viscosity-affected sub-layer (VASL) – is the subject of the present paper. In particular, we are concerned with how one should accurately model the flow in this region in a form suitable for use in CFD software.

However, accuracy is not the only criterion. The VASL, as implied above, is a region where effective transport properties change at a rate typically two or more orders of magnitude faster than elsewhere in the flow. So, if one adopts the same numerical strategy, a very much finer mesh is required. Consequently, while the VASL occupies no more than around 1% of the flow, just resolving that region requires between 3 and 300 times as much computing time (depending upon the flow problem, the complexity of the mathematical model of turbulence and the type of CFD solver adopted) as would be required if the mesh density could be kept comparable with that in the fully turbulent part of the flow.

Notwithstanding, despite the inevitably high computational cost, there has been a large effort in academic circles over the past forty years at developing models of turbulence that are applicable in both the fully turbulent regime and the viscous sub-layer – so-called low-Reynolds-number models. Models of this type range from the simple mixing-length schemes from the 1960's and two-equation eddy-viscosity models

(EVM's) from the 1970's through to more intricate connections between the turbulent fluxes and the mean-field gradients, exemplified by non-linear eddy-viscosity models (NLEVM's) and second-moment closures.

While models of this type have enabled accurate CFD computations to be made of a range of difficult flows, they are not the subject of this review (though results obtained with such models will be included in some of the later comparisons). Instead, attention is directed at much simpler approaches to handling the sub-layer region known as wall functions (Patankar and Spalding, 1967). Now, wall functions can be of many different types. Their aim, however, is to replace the difference equations solved on a very fine grid across the sub-layer by algebraic formulae or other low-cost routes that provide the overall resistance of the region to heat and momentum transport.

Wall-function strategies are certainly the approach preferred by commercial CFD code vendors and their clients. However, the accuracy that the adopted schemes return when applied to new types of problem is quite uncertain. As an illustration, Fig. 1 shows the computed heat-transfer coefficients produced by a range of different computors for the problem of convective heat transfer downstream from an abrupt pipe enlargement. Evidently, there are vastly different predicted variations of Nusselt number among the entries. While the example is not a recent one, the wall functions used and misused in those computations are still, for the most part, those in use today. It is thus timely that a reappraisal of practices should be undertaken.

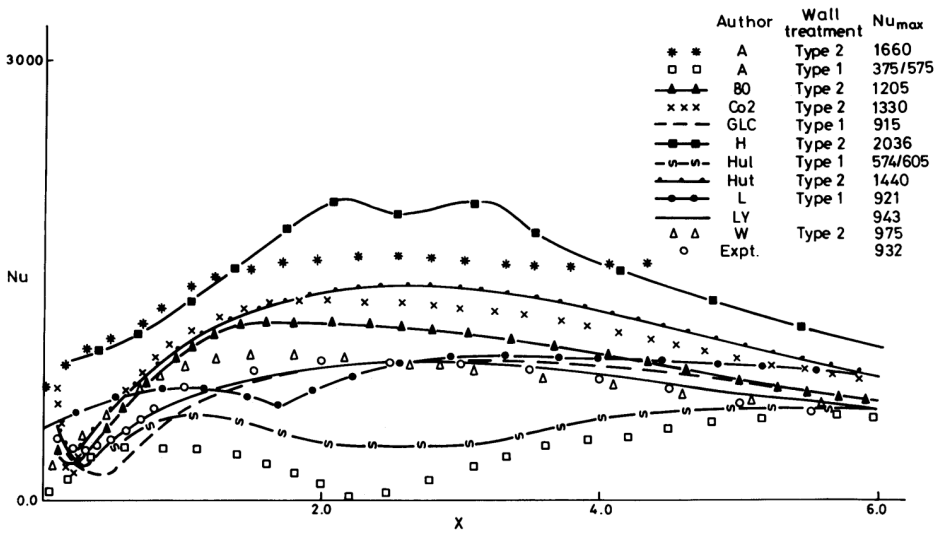

Figure 1: Nusselt number distributions downstream of an abrupt pipe enlargement submitted for an IAHR Workshop, 1987 (Personal communication, A.G. Hutton and R. Szczepura).

2 Essential Features of the VASL and Simple Approaches to its Modelling

Let us imagine a wall whose surface lies in the x-z plane with the mean velocity, U, in the x direction. At the wall itself, the no-slip condition requires that the fluctuating velocity components should vanish. Moreover, if the density may locally be assumed uniform, from continuity the fluctuating velocity gradient in the direction normal to the wall, y, must also vanish. Thus, if the velocity components are expanded in a Taylor series in terms of the wall-normal distance, we deduce that while the normal stresses $\overline{u^2}$ and $\overline{w^2}$ initially increase as y^2, $\overline{v^2}$, as signalled above, increases as y^4 (throughout the article *kinematic* stresses are employed with typical dimensions $(\mathrm{m/s})^2$). Equally important, the turbulent shear stress $\overline{uv}$ increases only as y^3. These different exponents of dependency on y have been well confirmed both by experiment and direct numerical simulation (Fig. 2).

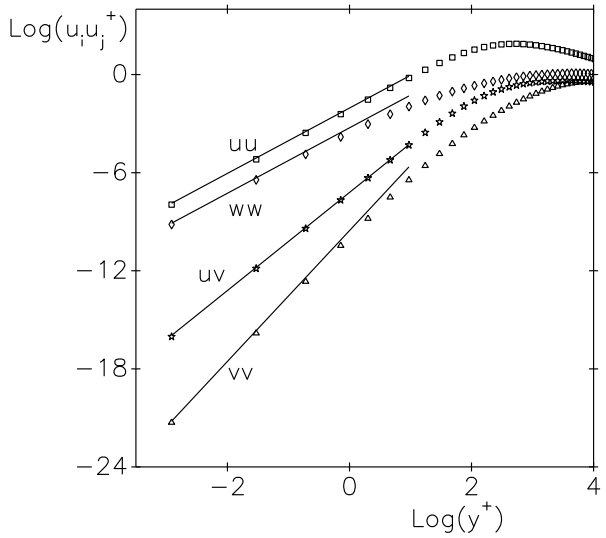

Figure 2: Near-wall variation of the Reynolds stresses. Symbols: DNS data (Kim et al., 1987); Solid lines are of slope 2 (for $\overline{u^2}$ and $\overline{w^2}$), 3 (for $\overline{uv}$) and 4 (for $\overline{v^2}$).

Because of the thinness of the sub-layer across which the changeover from molecular to turbulent transport occurs, in simple flows the shear stress parallel to the wall within the fluid is often essentially uniform and equal to the wall kinematic shear stress, τ_w/ρ. As one moves further from the wall there is a progressive switchover from molecular to turbulent stress as exemplified by the y^3 variation noted above. Now, as Reynolds' pioneering paper (Reynolds, 1895) first showed, the rate of conversion of mean kinetic energy into turbulent kinetic energy by mean shear is equal to $-\overline{uv}\,\partial U/\partial y$. In a constant stress layer this leads directly to the conclusion (Rotta, 1962) that the maximum rate of turbulence energy generation occurs where the turbulent and viscous stresses are equal i.e. where $\nu\,\partial U/\partial y = -\overline{uv} = {}^1\!/_2\tau_w/\rho$. That is why in simple wall shear flows the most intense turbulent velocity fluctuations normally appear within the VASL.

If the region adjacent to the wall may be supposed to be at constant shear stress then dimensional analysis readily suggests that within that region

$$U^+ \equiv U/U_\tau = f(y^+) \equiv f(yU_\tau/\nu) \tag{1}$$

where U_τ is the friction velocity $\sqrt{\tau_w/\rho}$. If the region of validity of Eq. (1) extends into the fully turbulent regime various arguments, ranging from the mixing-length hypothesis to Millikan's overlap concept (Millikan, 1939) may be employed to infer that there Eq. (1) may be particularized to:

$$U^+ = \frac{1}{\kappa}\ln(Ey^+) \tag{2}$$

where κ and E are regarded as universal constants. While κ, usually known as the von Karman constant, reflects the structure of turbulence in this 'fully turbulent' region, the coefficient E is dependent upon the flow structure over the VASL.

Equation (2) is of course very well known and has been used directly for applying effective wall boundary conditions in CFD methods to avoid having to resolve the viscous sub-layer, (Bradshaw et al., 1967). As such, it may be said to be the earliest 'wall function'. What is less extensively appreciated is how narrow the validity of this relationship is. The reason is that Eq. (1) (and hence Eq. (2)) is applicable only if the shear stress remains very nearly constant across the region to which it is applied. Even a decrease in shear stress across the sub-layer of just 5% causes a marked increase in the constant E in Eq. (2). Physically this amounts to a thickening, in terms of y^+, of the VASL due, ultimately, to the relative

decline of turbulence energy generation relative to viscous dissipation in the sub-layer. Such a decrease in shear stress may arise *inter alia* from flow acceleration (Jones and Launder, 1972a; Perkins and McEligot, 1975; Kays and Moffat, 1975); suction through the wall (Kays and Moffat, 1975); net buoyant force on vertical walls (Jackson and Hall, 1978) or, indeed, even in fully-developed pipe flow at bulk Reynolds numbers below 10^4 (Kudva and Sesonske, 1972; Patel and Head, 1969).

Likewise, a strongly increasing shear stress with distance from the wall (whether caused by an adverse pressure gradient or transpiration through a porous wall) can lead to a thinning of the sublayer, (Simpson et al., 1969; Spalart and Leonard, 1986; Launder, 1986). The picture is further complicated by flow impingement where turbulence energy is generated by the interaction of normal stresses and normal strains rather than by shear.

We shall shortly consider improvements on the basic form of velocity wall function but first let us note the thermal equivalent to Eq. (2):

$$\Theta^+ = \frac{1}{\tilde{\kappa}} \ln(\tilde{E} y^+) \tag{3}$$

where Θ^+ is the dimensionless temperature difference $(\Theta_w - \Theta)\rho U_\tau C_p / \dot{q}''_w$ and $\tilde{\kappa}$ and $\tilde{E}$ are the thermal counterparts of κ and E. Note, however, that $\tilde{E}$ depends on the Prandtl number of the fluid, σ. By introducing Eq. (2), Eq. (3) may be re-written

$$\Theta^+ = \frac{\kappa}{\tilde{\kappa}} U^+ + \frac{1}{\kappa} \ln(\tilde{E} y^+) \tag{4}$$

The ratio $\kappa/\tilde{\kappa}$ is essentially what is referred to as the *turbulent Prandtl number*, σ_t, and the result may thus be re-cast as

$$\Theta^+ = \sigma_t \left(U^+ + P\left(\frac{\sigma}{\sigma_t}\right)\right) \tag{5}$$

The quantity P (usually termed the Jayatilleke pee-function) can be determined from experimental data (Jayatilleke, 1969) or from analysis, assuming a distribution of turbulent viscosity and Prandtl number over the viscous region, (Spalding, 1967b; Patankar and Spalding, 1967).

A particularly simple form (Spalding, 1967b)

$$P \equiv 9.24 \left\{ \left(\frac{\sigma}{\sigma_t}\right)^{3/4} - \left(\frac{\sigma}{\sigma_t}\right)^{1/4} \right\} \tag{6}$$

has been widely adopted. As suggested by Eq. (6), P provides a measure of the different 'resistances' of the sub-layer to heat and momentum transport; when σ is less than σ_t, P is negative.

While, as noted, the presumption that the (dimensionless) viscous sub-layer was of universal thickness rendered the formulae discussed above of limited applicability even in simple shear flow, more serious weaknesses appeared in situations where the near-wall flow ceased to be shear dominated; for example, at separation or stagnation points. Then the use of the friction velocity, U_τ, as the normalizing velocity scale led to absurd results such as a zero heat transfer coefficient at a stagnation point! This weakness was partly removed (Spalding, 1967a; Gosman et al., 1969) by replacing U_τ in Eq. (2) by $c_\mu^{1/4} k_r^{1/2}$. Here k_r denotes the turbulent kinetic energy at a reference near-wall point in the fully turbulent region and c_μ is a constant (usually taken as 0.09). Thus, the conventional forms of Eqns. (2)–(3) are generalized to:

$$U^* = \frac{1}{\kappa^*} \ln(Ey^*) \tag{7}$$

$$\Theta^* = \sigma_t \left(U^* + P^*\right) \tag{8}$$

where

$$U^* \equiv \rho U k_r^{1/2}/\tau_w \qquad \Theta^* \equiv (\Theta_w - \Theta)\rho C_p k_r^{1/2}/\dot{q}_w''$$

and $\kappa^* \equiv c_\mu^{1/4}\kappa$; $E^* \equiv c_\mu^{-1/4}E$; $P^* \equiv c_\mu^{-1/4}P$.

Wall functions also need to be provided for any turbulence variables computed during the course of the computations, most usually for the turbulence energy, k, and its dissipation rate, ε. When turbulence in the fully turbulent near-wall region is in equilibrium, we may assume locally that the production and dissipation of turbulence energy are in balance. Thus for simple shear:

$$\varepsilon = -\overline{uv}\,\frac{\partial U}{\partial y} \tag{9}$$

This prescription is often used to fix ε at the near-wall node in boundary-layer (marching) solvers where the flow next to the wall is, indeed, often close to local equilibrium. The turbulent kinetic energy in these circumstances is likewise prescribed in terms of the wall shear stress

$$k = c_\mu^{-1/2}\tau_w/\rho \tag{10}$$

In separated flows, where local generation rates and the wall shear stress may be close to zero even though the near wall turbulence energy may be large, these practices are inadequate. This includes most situations where heat-transfer rates are of interest. Here the practice usually followed is to solve the budget equation for k assuming zero diffusion of turbulence energy to the wall (reasonable since k varies as y^2 at the wall and its transport is driven by molecular diffusion). The most complete statement of this approach is given by (Chieng and Launder, 1980). A crucial element lies in deciding the average generation and dissipation rates over the near-wall-cell since the variation of each is highly non-linear. For a cell extending to a height y_n from the wall, the average generation rate of turbulence energy, presuming the generation arises simply from shearing, is

$$\overline{P} = -\frac{1}{y_n}\int_0^{y_n} \overline{uv}\,\frac{dU}{dy}\,dy \tag{11}$$

Too often, in the above, $(-\overline{uv})$ is replaced by τ_w/ρ which leads to the attractively simple but incorrect result

$$\overline{P} = \frac{\tau_w U_n}{\rho\, y_n} \tag{12}$$

The problem with the above is that within the truly viscous sub-layer the shear stress is transmitted by molecular interactions, not by turbulence, and there is no creation of turbulence linked with the (usually) intense velocity gradient there. What one should have is

$$\overline{P} = \frac{\tau_w (U_n - U_v)}{\rho\, y_n} \tag{13}$$

The above result is based on the simple notion that there is an abrupt changeover from molecular to turbulent transport at a distance y_v from the wall. A corresponding strategy is applied to obtain the mean energy dissipation rate, $\overline{\varepsilon}$. In this case (as detailed in Section 3) within the sub-layer, the local dissipation rate is not zero. Indeed, DNS studies of near-wall turbulence usually show that the maximum

value occurs at the wall itself. These features were adopted in wall functions (Chieng and Launder, 1980; Johnson and Launder, 1982) but it was found that, typically, the level of Nu in separated flows was underestimated by 20-30%. Reasonable accord with experiment was achieved, however, by allowing the sub-layer to become thinner when there was a substantial diffusive influx of turbulent kinetic energy towards the wall, broadly in line with earlier experimental observations noted above.

Amano developed a more elaborate wall-function treatment (Amano, 1984) by decomposing the viscosity-affected zone into a laminar sub-layer and a buffer region where turbulent transport was increasingly important as one proceeded away from the wall. Another significant difference was his practice of determining the near-wall value of $\overline{\varepsilon}$ from its transport equation rather than by prescribing the length scale. He examined similar pipe-expansion test flows to (Johnson and Launder, 1982) but concluded that his 2-layer viscous/buffer model gave satisfactory agreement with experiment whereas the Chieng-Launder single-layer version produced too *high* values of Nu even though, in representing the velocity field, he adhered to a constant dimensionless sub-layer thickness. The reason for this strikingly different behaviour from that reported in (Johnson and Launder, 1982) was probably linked with the necessarily crude, coarse-grid approximation of the source-terms in the ε-equation over the near-wall cell.

Finally, (Ciofalo and Collins, 1989) confirmed the conclusion of (Johnson and Launder, 1982) that the variation of the sub-layer thickness was, indeed, a vital element of any wall treatment for impinging or separated flows. However, they related the sub-layer thickness not to the diffusive inflow of turbulence energy but to the local turbulence intensity, $k^{1/2}/U$, at the near-wall node, a practice that, from a numerical point of view, was certainly more stable.

3 Two Current Approaches

For at least ten years preceding the work summarized below there seems to have been little, if any, work directed at improving wall-function practices, at least within the context of RANS computations. The available schemes were, however, plainly deficient on various counts.

At UMIST, from 1999, two PhD projects have been focused on developing more general wall-functions. Each has adopted a quite different pathway. In what follows a brief account will be provided of both routes, one an analytical scheme, UMIST-A (Unified Methodology for Integrated Sub-layer Transport - Analytical), the other numerical (UMIST-N). While the latter scheme is the more general, the former is more evidently an evolution of the practices reported in Section 2. It also provides a clear, albeit simple, physical model based on an analytical solution of the streamwise momentum and energy equations in the near-wall region. It was commissioned for use in safety studies by a consortium of UK nuclear-power companies who were concerned that available wall functions did not permit a realistic representation of the near-wall flow under mixed or natural-convection conditions such as may arise following a failure of the reactor circulation pumps. Specifically the approach should be able to cope with:

- forced, mixed or natural convection flow on near vertical surfaces,
- strong variations of molecular transport properties across the VASL,
- laminarization, i.e. a marked thickening of the VASL in buoyancy-aided mixed convection.

A detailed account of the resultant scheme has been published (Craft et al., 2002) and here just the main elements that especially relate to the above capabilities are noted. The starting point is a prescribed ramp distribution of turbulent viscosity, Fig. 3a:

$$\frac{\mu_t}{\mu_v} = c_\mu c_l \left(y^* - y_v^*\right) \quad \text{for } y^* \geq y_v^* \tag{14}$$

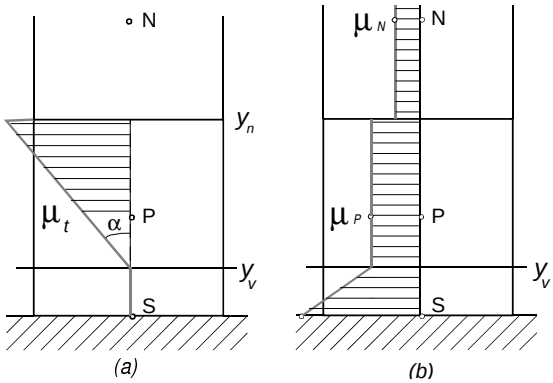

Figure 3: Viscosity distributions assumed over near-wall cell. a) Turbulent viscosity. b) Molecular viscosity.

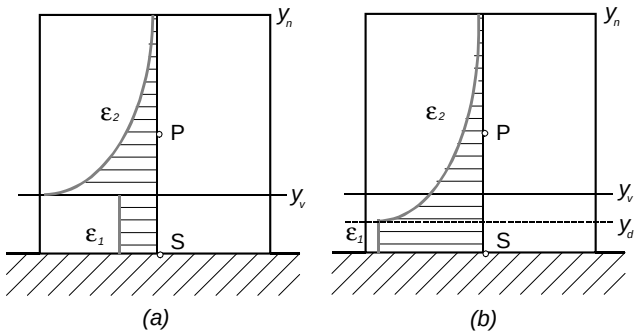

Figure 4: Distribution of ε over near-wall cell. a) Conventional prescription, (Chieng and Launder, 1980). b) Currently adopted variation.

The coefficients c_μ and c_l are the conventional ones adopted in 1-equation turbulence models (0.09, 2.55) where now $y^* \equiv \rho_v y k_P^{1/2}/\mu_v$ and the subscript denotes where the quantity is evaluated: 'v' – at the edge of the viscous layer; 'P' – at the near-wall node. This rather simple viscosity profile was essential to retain a form amenable to integration of the differential equations to obtain velocity and temperature profiles, including the case where buoyant effects were significant. Initially it was intended to evaluate k in the definition of y^* at the sub-layer interface, y_v, as proposed in (Chieng and Launder, 1980). However, this proved a much less stable practice than adopting the nodal value and, surprisingly, it also led to greater dependence on the size of the near-wall cell. (The reason seems to be that to extrapolate to y_v requires the use of information further from the wall than y_P).

In flows with intense wall heating some account of the variation of molecular properties across the sub-layer needs to be taken, Fig. 3b. The way this is done profoundly affects the numerical stability of the equation set. First it was found preferable to cast the dependence in terms of y^* rather than of temperature. Secondly, while a linear variation was tried, this turned out to be much less stable than a hyperbolic variation:

$$\mu = \frac{\mu_v}{1 + b_\mu \left(y^* - y_v^*\right)} \tag{15}$$

where $b_\mu = (\mu_{wall} - \mu_v)/(y_v^* \, \mu_{wall})$.

Another area where it was felt appropriate to improve current practice was in the prescription of the kinetic energy dissipation rate next to the wall, Fig. 4. (Chieng and Launder, 1980) had approximated the exact result (Jones and Launder, 1972b)

$$\varepsilon_v = \nu \left(\frac{\partial k^{1/2}}{\partial y} \right)^2 \approx \frac{2\nu k}{y^2} = \frac{2\nu k_P}{y_v^2} \tag{16}$$

However, while k varies parabolically with y very close to the wall, it levels out near the point of maximum k-production. Consequently, the last form in Eq. (16) gave sub-layer dissipation levels lower than that in the adjacent fully-turbulent zone, a result which was at odds with all DNS data. To correct this anomaly it was supposed that the sub-layer for the dissipation rate was smaller than y_v, the distance being chosen so that the dissipation rates in the two zones were equal at $y = y_d$:

$$\varepsilon_w = \frac{2\nu k_P}{y_d^2} = \frac{k_P^{3/2}}{c_l \, y_d} \tag{17}$$

In fact, the choice of smaller y_d than y_v has been made in a number of the low-Reynolds-number turbulence models (Wolfshtein, 1969). The mean value of ε over the inner cell is obtained by integration over the near-wall control volume as in (Chieng and Launder, 1980; Ciofalo and Collins, 1989).

To make the treatment sensitive to laminarization two choices had to be made, namely, the most appropriate parameters as *detector* and *operand*. We concluded, in line with some of the earlier mixing-length models, that the ratio of the shear stress between the wall and the edge of the sub-layer, λ, was the best detector. Initially we attempted to correlate y_v^* as a function of this parameter but this proved to have poor stability characteristics. Accordingly, a more direct choice for the operand was adopted: the mean level of dissipation rate over the near-wall control volume (obtained as noted in the preceding paragraph) was adjusted by a weighting function F_ε that in turn was a function of λ:

$$\overline{\varepsilon}_{new} = F_\varepsilon(\lambda)\,\overline{\varepsilon}_{old} \tag{18}$$

Other features of the overall scheme to note are that:

- Convective transport (which is ignored in many wall-function treatments) is retained in simplified form.
- When buoyancy is important the buoyant force in the vertical momentum equation is obtained by integrating a fit to the analytical temperature profile over the cell rather than basing the force purely on the temperature at the near-wall node itself.
- When the viscous sub-layer thickness exceeds the cell thickness, y_n, (as it may do in limited regions if a structured grid is adopted) a reformulation is needed based on identical principles.

These and other features of the scheme are detailed in (Craft et al., 2002).

Figures 5–6 provide an impression of the capabilities of the method. Figure 5 shows, for a low-Reynolds-number pipe flow, the variation of velocity on wall-law axes. We note that the experimental data of (Kudva and Sesonske, 1972) lie above the supposedly 'universal' log law as do predictions with the low-Reynolds-number (LRN) k-ε model of (Launder and Sharma, 1974). More importantly, the present wall-function results also accord with the data and, in contrast to most such schemes, show scarcely any sensitivity to the size of the near-wall cell. As a second example, Fig. 6 relates to upflow in a vertical pipe where, at $x/d = 50$, strong uniform heating is applied at the wall causing a buoyant upthrust on the near-wall fluid which thus accelerates. This causes a marked drop in Nusselt number below the Dittus-Boelter correlation, shown by the solid horizontal line. Again, the wall-function results accord well with the data. For one run the $F_\varepsilon(\lambda)$ correction was not applied and this evidently leads to a 20% increase in Nusselt number. Further applications of the above strategy are given in (Craft et al., 2002).

A type of flow for which the above analytical approach is not equipped is where the velocity profile parallel with the wall undergoes strong skewing across the sublayer, as it does, for example, in the oblique impingement of flow on a bank of heat-exchanger tubes. Moreover, for flow with strong streamline curvature, it is known that the linear stress-strain relation adopted in eddy viscosity models does not adequately mimic the turbulence-generation processes. In view of the above difficulties, a different strategy has been evolved, UMIST-N. In form it is much more akin to low-Reynolds-number models in that the wall-function cell is itself sub-divided into, typically, 40 thin slices, Fig. 7. The mean flow and turbulence differential equations, suitably simplified, are solved on this fine grid in order to generate the data required as "wall-function" quantities to supply appropriate wall boundary conditions for the whole-field solution carried out on the primary grid.

Of course, as noted, simplifications are made to the equations solved on the fine grid in order to secure the great reduction in computer time that one seeks from wall functions. Firstly, the pressure gradient parallel to the wall is assumed uniform across all the sub-grids, equal to the pressure gradient across

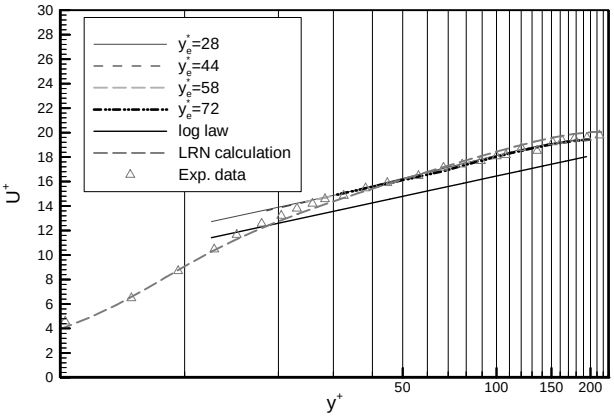

Figure 5: Mean velocity profile in pipe flow in wall-layer coordinates, $Re = 6753$. Symbols: experiments (Kudva and Sesonske, 1972); Solid line: log-law; Light broken line: LRN calculation; Other lines: UMIST-A.

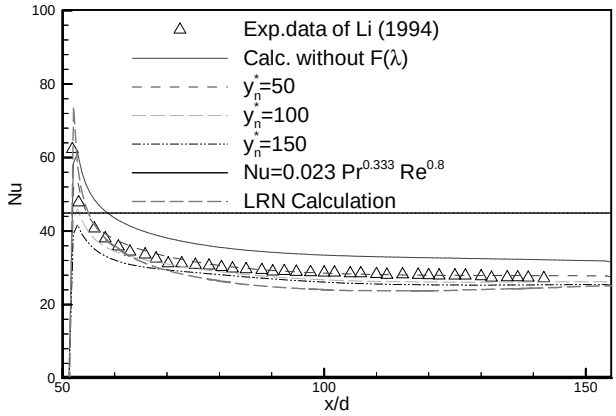

Figure 6: Variation of Nusselt number in mixed-convection upflow in a vertical tube. Symbols: experiments (Li, 1994); Solid line: Dittus-Boelter; Medium broken line: LRN calculation; Dotted line: UMIST-A without $F_\varepsilon(\lambda)$; Other lines: full UMIST-A treatment.

the near-wall cell of the primary grid. Moreover, the velocity component normal to the wall is found by continuity rather than by solving the momentum equation normal to the wall. In these respects the fine-grid solution is essentially obtained with a separate boundary-layer solver. It is, however, applied simply to the immediate near-wall layer extending to values of y^* of 100 or less. Boundary conditions imposed at the outer edge of the subgrid at $y = y_n$ are simply interpolated from values held on the primary grid at y_P and y_N. At the wall itself the same boundary conditions are applied as for a conventional treatment of a LRN model, including zero values for the mean velocity components and k.

Two alternative turbulence models have been employed within the above numerical treatment: the LRN k-ε model (Launder and Sharma, 1974) and a cubic non-linear eddy viscosity model (Craft et al., 1996). The cubic terms in the latter model make it far more sensitive to streamline curvature than a linear EVM. The first test case is for a turbulent jet impinging orthogonally onto a flat, uniformly heated plate. The jet discharges from a long smooth pipe whose exit is four diameters above the plate. Figure 8 shows the resultant variation of Nusselt number over the plate from the stagnation point ($r = 0$) outwards. In fact, linear eddy viscosity models do a poor job at reproducing impinging flows because of the very different strain field than found in simple shear. As is seen in Fig. 8a, the computed Nusselt number at the stagnation point is more than twice the measured value. However, at least the wall-function solutions are

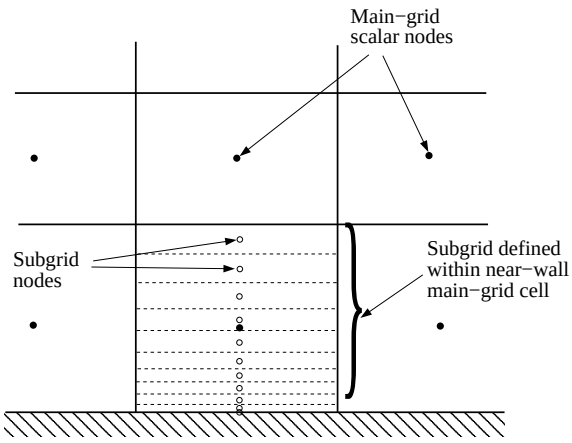

Figure 7: Treatment of near-wall control volume in UMIST-N.

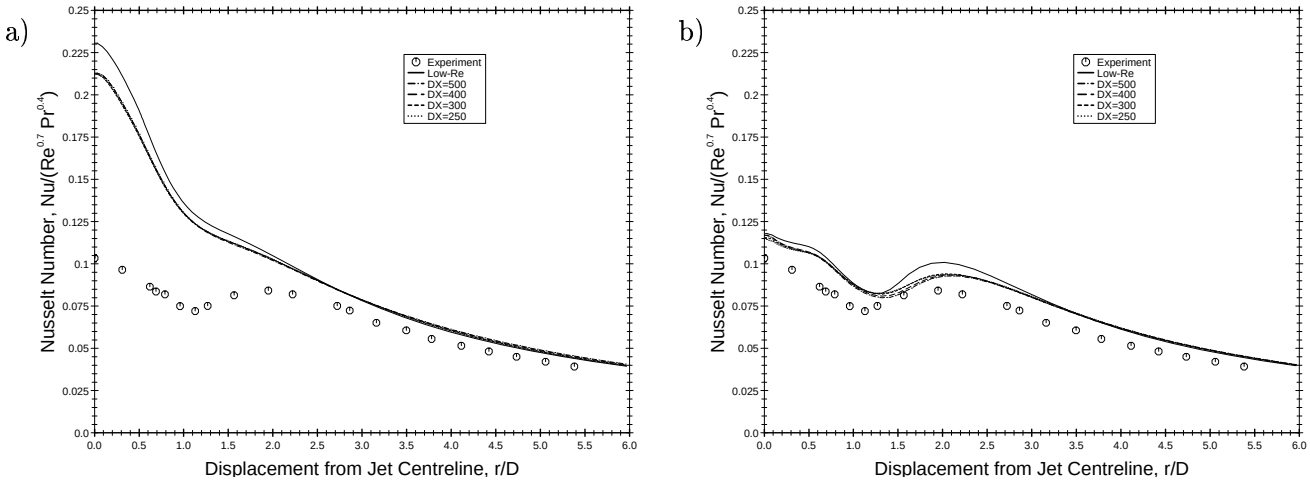

Figure 8: Nusselt number variation on a flat plate beneath an axisymmetric impinging jet. a) Linear k-ε EVM. b) Cubic non-linear EVM (Craft et al., 1996). Symbols: experiments (Baughn et al., 1992); Heavy line: full LRN treatment; Other lines: UMIST-N.

in close accord with the complete LRN computations: in other words the much simplified treatment over the near-wall cell has had only a very minor effect on the computed Nusselt number. Figure 8b presents results for the same test flow but where the non-linear EVM (Craft et al., 1996) is adopted. Agreement with experiment is now much closer and, as with the linear EVM, there is close accord between the wall-function and complete LRN treatments. Note too that there is scarcely any sensitivity to the thickness of the "wall-function" region, which is a very desirable characteristic. The only major difference between the UMIST-N results and those of the complete LRN treatment is in the computer time required: the wall-function result with the same grid density takes less than one eighth of the time required for the complete numerical model.

As a final example we consider heat transfer from a mildly heated disc spinning about its own axis. The disc's rotation induces a radially outward motion that peaks outside the VASL. The tangential velocity, by contrast, increases rapidly across the sublayer to Ωr on the disc surface (Ω the disc's angular velocity and r the local radius). Hence, the mean velocity vector undergoes severe skewing across the VASL. This effect is satisfactorily reproduced by virtually any LRN model but cannot be accounted for with conventional wall functions (including UMIST-A) which, with the wall-adjacent node in the turbulent region, incorrectly take the wall shear stress to point in the same direction as the near-wall velocity vector. Figure 9, however, shows that the induced radial velocity predicted with the numerical wall function (using the linear EVM of (Launder and Sharma, 1974)) agrees very closely with the results of the corresponding LRN computation. The integral Nusselt number in Fig. 10 also shows negligible differences among the alternative treatments: all the computations reproduce the experimental data with reasonable fidelity. In this case, for equivalent grids and convergence limits, the complete low-Reynolds-number model required thirteen times more computation time than UMIST-N!

As a final observation on both the wall-function approaches outlined in this section, all the applications so far considered are relatively straightforward compared with the types of flows the industrial user needs to compute. However, we see no evident impediment to their use in these more complex flows. Indeed, we hope that the turbulent-flow CFD community will contribute to this wider testing and, where necessary, the improvement of these prototype forms.

Acknowledgements: The research summarized in Section 3 has been supported by British Energy, plc and the UK Engineering & Physical Sciences Research Council. Mrs P. Shepherd has assisted in preparing the camera-ready manuscript. Authors' names are listed alphabetically.

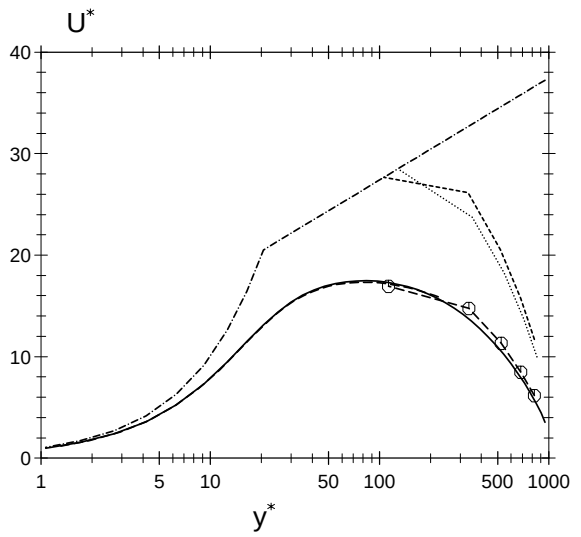

Figure 9: Radial velocity profile for spinning disc in wall-layer coordinates. Solid line: LRN calculation; Broken line with symbols: UMIST-N; Chain line: log-law; Other lines: standard wall-function treatments.

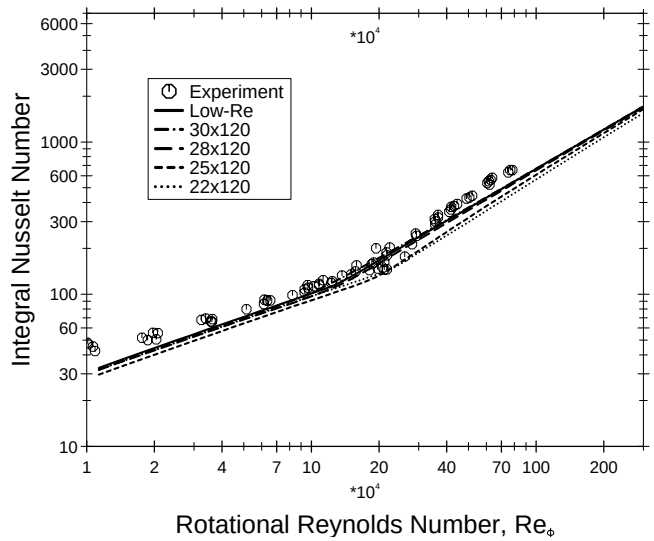

Figure 10: Variation of Nusselt number for spinning disc with Reynolds number. Symbols: experiment (Cobb and Saunders, 1956); Heavy line: Full LRN treatment; Other lines: UMIST-N.

References

R. Amano, Development of a turbulence near-wall model and its application to separated and reattached flows, Numerical Heat Transfer, vol. 7, pp. 59–76, 1984.

J. W. Baughn, X. Yan and M. Mesbah, The effect of Reynolds number on the heat transfer distribution from a flat plate to an impinging jet, in ASME Winter Annual Meeting, 1992.

P. Bradshaw, D. H. Ferriss and N. P. Attwell, J. Fluid Mech., vol. 29, p. 625, 1967.

C. C. Chieng and B. E. Launder, On the calculation of turbulent heat transport downstream from an abrupt pipe expansion, Numerical Heat Transfer, vol. 3, pp. 189–207, 1980.

M. Ciofalo and M. W. Collins, k-ε predictions of heat transfer in turbulent recirculating flows using an improved wall treatment, Numerical Heat Transfer, vol. 15, pp. 21–47, 1989.

E. C. Cobb and O. A. Saunders, Heat transfer from a rotating disk, Proc. Roy. Soc. Lond. A, vol. 236, pp. 343–351, 1956.

T. J. Craft, A. V. Gerasimov, H. Iacovides and B. E. Launder, Progress in the generalization of wall-function treatments, Int. J. Heat Flow Flow, vol. 23, pp. 148–160, 2002.

T. J. Craft, B. E. Launder and K. Suga, Development and application of a cubic eddy-viscosity model of turbulence, Int. J. Heat and Fluid Flow, vol. 17, pp. 108–115, 1996.

A. D. Gosman, W. M. Pun, A. K. Runchal, D. B. Spalding and M. Wolfshtein, Heat and mass transfer in recirculating flows, Academic, London, 1969.

J. D. Jackson and W. B. Hall, Forced convection heat transfer to supercritical-pressure fluids, in NATO Advanced Studies Institute, Bogazia University, Istanbul, 1978.

C. L. V. Jayatilleke, The influence of Prandtl number and surface roughness on the resistance of the laminar sublayer to momentum and heat transfer, Prog. Heat Mass Transfer, vol. 1, p. 193, 1969.

R. W. Johnson and B. E. Launder, Discussion of 'On the calculation of turbulent heat transport downstream from an abrupt pipe expansion', Numerical Heat Transfer, vol. 5, pp. 493–496, 1982.

W. P. Jones and B. E. Launder, J. Fluid Mech., vol. 56, p. 337, 1972a.

W. P. Jones and B. E. Launder, The prediction of laminarization with a two-equation model of turbulence, Int. J. Heat Mass Transfer, vol. 15, pp. 301–314, 1972b.

W. M. Kays and R. J. Moffat, Studies in convection, vol. 1, Academic, 1975.

J. Kim, P. Moin and R. Moser, Turbulence statistics in fully developed channel flow at low Reynolds number, J. Fluid Mech., vol. 177, pp. 133–166, 1987.

A. A. Kudva and A. Sesonske, Structure of turbulent velocity and temperature fields in ethylene glycol pipe flow at low Reynolds number, Int. J. Heat Mass Transfer, vol. 15, p. 127, 1972.

B. E. Launder, Low-Reynolds-number turbulence near walls, Tech. Rep. Report TFD/86/4, Department of Mechanical Engineering, UMIST, 1986.

B. E. Launder and B. I. Sharma, Application of the energy-dissipation model of turbulence to the calculation of flow near a spinning disc, Lett. in Heat Mass Transfer, vol. 1, pp. 131–138, 1974.

J. Li, Studies of buoyancy-influenced convective heat transfer to air in a vertical tube, Ph.D. thesis, University of Manchester, 1994.

C. B. Millikan, A critical discussion of turbulent flows in channels and circular tubes, in Proc. 5th Int. Congress for Appl. Mech., pp. 386–392, 1939.

S. V. Patankar and D. B. Spalding, Heat and mass transfer in boundary layers, 1st edn., Morgan Grampian Press, 1967.

V. C. Patel and M. R. Head, J. Fluid Mech., vol. 38, p. 181, 1969.

K. R. Perkins and D. M. McEligot, ASME J. Heat Trans., vol. 97, p. 589, 1975.

O. Reynolds, On the dynamical theory of incompressible viscous fluids and the determination of the criterion, Phil. Trans. Roy. Soc. A, vol. 186, pp. 123–164, 1895.

J. C. Rotta, in D. Kuchemann (ed.), Progress in the aeronautical sciences, 1962.

R. L. Simpson, W. M. Kays and R. J. Moffat, Tech. Rep. Report HMT-2, Mech. Eng. Dept., Stanford University, 1969.

P. Spalart and A. Leonard, Direct numerical simulation of equilibrium turbulent boundary layers, in F. J. Durst et al (ed.), Turbulent Shear Flows – 5, Springer Verlag Heidelberg, 1986.

D. B. Spalding, Heat transfer from turbulent separated flows, J. Fluid Mech., vol. 27, p. 97, 1967a.

D. B. Spalding, Monograph on turbulent boundary layers, Chapter 2, Tech. Rep. Rep. TWF/TN/33, Imperial College Mech. Eng. Dept., 1967b.

M. Wolfshtein, The velocity and temperature distribution in one-dimensional flow with turbulence augmentation and pressure gradient, Int. J. Heat Mass Transfer, vol. 12, pp. 301–318, 1969.